

Harnessing Capacitance for Inter-Robot Latching, Communication, and Power Transfer

Mustafa Emre Karagozler

A report submitted in partial fulfillment of the requirements
for the degree of

Master of Science

in

Electrical and Computer Engineering

May 2007

Department of Electrical and Computer Engineering

Carnegie Mellon University

Pittsburgh, PA, 15232

ABSTRACT

A simple and robust inter-module latch is possibly the most important component of a modular robotic system. This report describes a latch based on capacitive coupling which not only provides significant adhesion forces, but can also be used for inter-module power transmission and communication. The key insight that enables electrostatic adhesion to be effective at the macro scale is to combine flexible electrodes with a geometry that uses shear forces to provide adhesion. To measure the effectiveness of our latch we incorporated it into a 28cm x 28cm x 28cm modular robot. The result is a latch which requires almost zero static power and yet can hold over $0.6N/cm^2$ of latch area.

ACKNOWLEDGMENTS

I would like to thank my adviser Prof. Seth C. Goldstein for his guidance and encouragement during the course of this work. His creative questioning led to many ideas that are presented in this report. I would also like to thank Prof. Gary K. Fedder for his insightful comments and taking out his time from his busy schedule to read this report.

I would like to thank Claytronics group members for insightful discussions. Michael P. Weller and Brian Kirby deserve special thanks for helping me with the prototype. I would also like to thank Jason Campbell and Byung Woo Yoon for their helpful comments.

Finally, I would like to thank my family and friends for their love and moral support.

CONTENTS

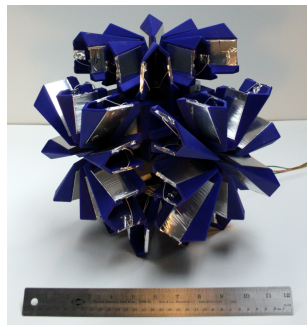
1. <i>Introduction</i>	5
2. <i>An Electrostatic Latch</i>	8
2.1 Implementation of a Macro-scale Electrostatic Latch	10
2.2 Evaluation of the Macro-scale Electrostatic Latch	14
2.3 Electrostatic Latches at the Micro-scale	16
2.4 Summary	19
3. <i>Power Transfer</i>	21
3.1 Feasibility of Power Transfer	21
3.2 Summary	27
4. <i>Demonstration Cubic Robot</i>	29
4.1 Actuation Subsystems	29
4.1.1 Mechanical Actuation for Expansion and Contraction	30
4.1.2 Genderless Self-aligning Comb Latch	30
4.2 Impact of Latch on Overall Design	30
4.3 Summary	32
5. <i>Conclusions</i>	33

1. INTRODUCTION

Modular robotics offers the tempting prospect of robotic systems which can be simultaneously cost-effective, robust, and yet flexible. Since early work on CEBOT [3] there have been numerous research projects aimed at realizing this promise (see [8] for a recent survey). Despite the significant progress that has been made in the past 15 years, creating a robust modular robotic system still poses significant engineering challenges. One key challenge to scaling modular robot ensembles beyond tens of units is the realization of a strong, lightweight, robust, manufacturable inter-module latching mechanism. In this report we describe a novel modular robot latch based on electrostatic attraction. Our latch design is suitable for lattice style robots at both the micro- and macro-scale.

An ideal inter-module latch provides structural stability, power distribution, and communication channels between the robots. It is self-aligning, genderless, and can engage/disengage easily and quickly. It weighs little with respect to the rest of the robot and does not consume any power to maintain a connection once it has latched. To date, latch design has required significant compromises with respect to the desired behavior. Latches are often heavy, take up significant amounts of space, require many seconds to engage, or provide only some of the desired capabilities. For example, the latch on the ATRON robot is one of the sturdiest implemented [8]. However, it accounts for well over half of each module's volume and weight.

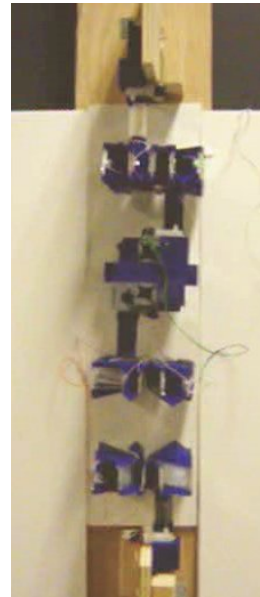
In the past, latches for centimeter-scale robots have been based upon either mechanical engagement (e.g., [8, 5, 10, 13, 9]) or magnetic forces (e.g., [12, 7, 6]). Electric field adhesion has been studied only for systems no larger than the millimeter-scale. In 2006, we experimented with electrostatic latches for a short-lived robot that we called a "giant helium catom" (GHC) [4]. The GHC was an $8m^3$ cube filled with helium to offset most of its weight and emulate the high surface area to weight ratios likely for sub millimeter-scale robot modules. The GHC latching mechanism was based upon electrostatic attraction between the faces of



(a) A fully contracted unit.



(b) A fully extended unit.



(c) In the test jig.

Fig. 1.1: Electrostatic-based modular robots. Related pictures and video can be found at www.cs.cmu.edu/~claytronics/iros07-latch.html

two adjacent cubes. While in theory the expected forces (given the large area of the faces) should have been sufficient to latch two robots together, the mechanism failed due to *peeling* (see Chapter 2). This failure led us to a new latch design that harnesses *shear forces* rather than normal forces. This change in force orientation eliminated the fatal peeling found in the GHC mechanism. Our current prototype of this new design can generate holding force of more than $0.6N/cm^2$ of latch area, when actuated with a voltage of $500V$.

When one mechanism can serve two or more purposes, the total weight, volume, and complexity requirements for a module can be reduced, allowing higher performance and improved scaling. The design of an electrostatic latch is simple, yet multipurpose: each robot has two halves of a capacitor on its face, and when faces from neighboring robots come in contact the pair of capacitors is complete. Viewing the latch as a pair of capacitors naturally leads to the idea of using these capacitors as a power and communication link between the robots. We detail our investigations in power transfer in Chapter 3.

In this report we demonstrate an electrostatic latch on a prototype modular robot modeled after the Crystalline Atom [9] and TeleCube [12]. The modules attach in a cubic lattice using electrostatic latches, and move their faces via expanding arms nested in the central frame, as shown in Figure 1.1a and b. This modular robot design is covered in more detail in Chapter 4.

2. AN ELECTROSTATIC LATCH

An ideal modular robotic latch should:

- have a high adhesion force when locked,
- lock and unlock easily,
- be self aligning,
- use minimal power during locking and unlocking,
- use no power once locked.

One approach to satisfying these requirements might be to use the electrostatic forces between the plates of a parallel plate capacitor as the basis for a latch. If the plates are close together, then when the capacitor is charged using a voltage source, large electrostatic forces will be generated between the plates of the capacitor—locking the latch. To unlock the latch, the capacitor is discharged. In addition, once the capacitor is charged, the charge remains to keep the latch closed indefinitely (neglecting leakage)— in other words, the latch uses no static power to remain attached.

Such a latch, modeled as a parallel plate capacitor, is shown in Figure 2.1. For electrical insulation, the conductive plates are separated by a thin dielectric film on each of them. For practical systems there will also be some intervening gap between the electrodes. The capacitance and the electrostatic force for the corresponding model are:

$$C = \frac{A\epsilon_0}{(l + 2d/\epsilon_r)}, \quad F = \frac{A\epsilon_0 V^2}{2(l + 2d/\epsilon_r)^2} \quad (2.1)$$

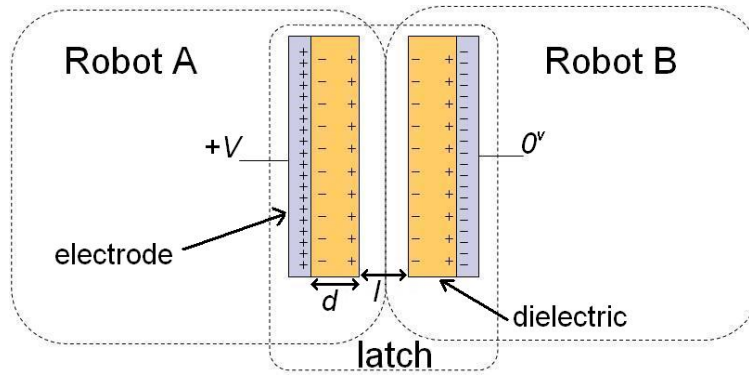


Fig. 2.1: Electrodes are aligned, forming the latch.

where A is the surface area of the electrodes, V is the applied voltage, d is the thickness of the dielectric coating, l is the separation between electrodes, ϵ_0 is the dielectric permittivity of vacuum and ϵ_r is the relative permittivity of the dielectric coating.

The electrostatic force heavily depends on the separation between the electrodes. For tens of Newtons of electrostatic force over an area of hundreds of cm^2 , the separation between the electrodes must be on the order of microns. Furthermore, because of the inverse-square relationship between electrostatic force F and inter-electrode distance l , an additional separation of only a few more microns will significantly reduce the generated force. However, when the electrodes are made out of rigid conductors (e.g., thick aluminum plates), even small levels of surface asperity (roughness) or dirt prevent the required close engagement. Rigid structures at this scale simply can not be made flat enough to be practical. Mechanical compliance, or flexibility of the electrodes offers a way to achieve closer spacing and obtain a large electrostatic force.

When flexible electrodes are charged, even if the initial separation is large, the (much smaller) electrostatic force developed can cause the electrodes to bend and more closely approach one another, reducing the separation and allowing larger electrostatic forces to be created. As a result of this mechanism, the flexible electrodes move toward each other until they completely conform to each other, resulting in significant adhesion forces.

However, flexible electrodes suffer from an effect we call *peeling* (see Figure 2.2) which limits the amount of adhesion that can be sustained. Flexibility means that portions of the electrodes' surfaces at the boundary contact can be separated without (much) impact on the separation of the rest of the surface (see

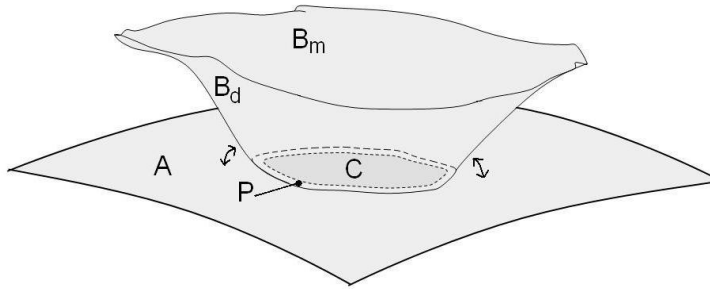


Fig. 2.2: Two flexible electrodes conforming onto each other: *A*: Bottom electrode, $B_{m,d}$ = Top electrode metal and dielectric side, *C*: Contact area, *P*: Boundary of contact.

regions *P* and *C* in Figure 2.2). Working incrementally, even a small force can then detach one electrode from another much like unzipping a zipper.

By reorienting the electrostatic force in the latch to run along the surface of each electrode rather than normal to it (i.e., to attempt to shear or drag each pair of electrodes), we can eliminate the potential for peeling. In the shear direction a force must act on the entire surface area at once. Careful design of electrode geometries can maximize the use of shear force and minimize the use of normal force.

Our latch design is based on shear forces. The contact surface of the electrodes is parallel to the direction of latch engagement. Thus, when the latch engages and locks, the shear force due to friction created by the electrostatic adhesion holds the latch together.

2.1 Implementation of a Macro-scale Electrostatic Latch

Each latch is composed of two genderless *faces* (Figure 2.3). In our prototype latch, a face is a star shaped plastic frame to which the electrodes are attached. Each face carries multiple electrodes, and each electrode is made from a thin aluminum foil + dielectric film wrapped and glued onto a plastic panel. The completed electrodes (panel+film) then slide into the corrugated star shaped face as shown in Figure 2.4. The face has both the normal surfaces necessary to create shear forces, and also gives the latch the ability to self-align. As the faces engage (Figure 2.5), the faces are guided both translationally and rotationally into position by the face shape, correcting any initial misalignment.

The latch is locked when a voltage is applied between the electrodes of the two faces. However, since

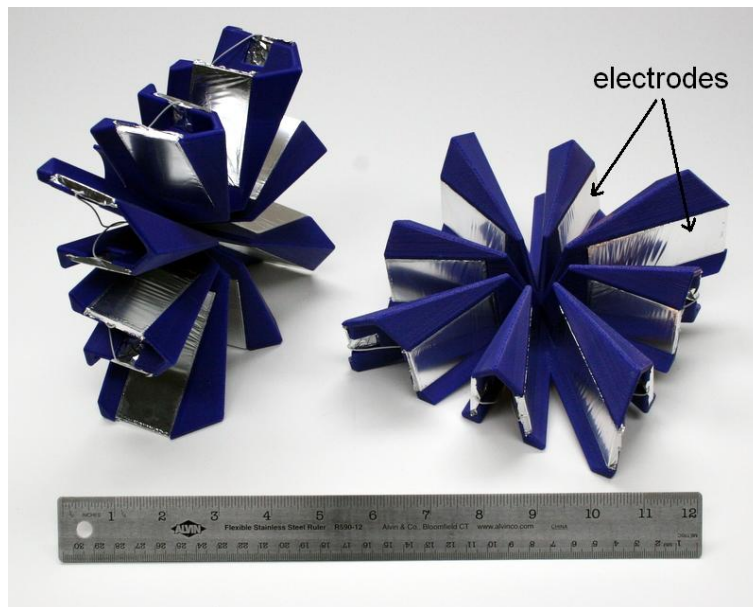


Fig. 2.3: A latch, composed of two faces.



Fig. 2.4: The electrodes slide into slots on the star shaped face.

each face of the latch is located on a different robot, the electrodes cannot share a common ground as in Figure 2.6a. Having multiple electrodes allows for various alternative ways to excite the latch. As shown in Figure 2.6b, the latch can be excited by applying a voltage difference on electrodes of only one face, while the other face is passive. Figure 2.6c shows another connection diagram where there is a voltage source on

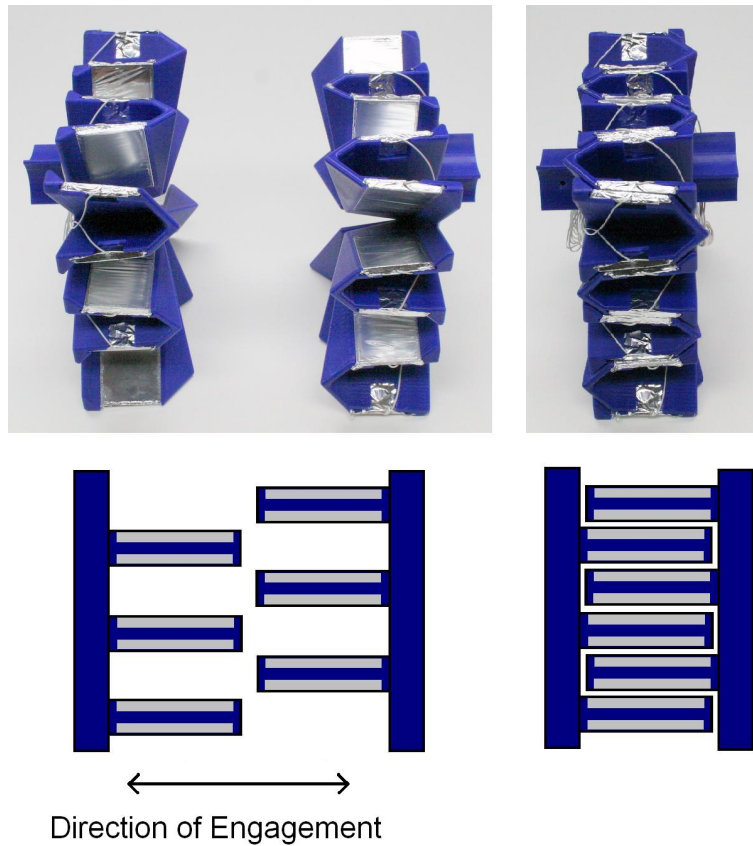


Fig. 2.5: The two faces of the latch engaging.

both faces, effectively increasing the voltage drop on each individual electrode pair by a factor of two. This increases the generated force by a factor of four. Also, as explained in Chapter 3, some of the electrodes can be dedicated to power transfer or communication, as shown in Figure 2.6d.

One face of our current latch prototype is $16\text{cm} \times 16\text{cm} \times 6\text{cm}$ in overall dimensions. The aluminum foil used is 20nm thick and the dielectric (mylar) coating of the foil is $6\mu\text{m}$ thick¹. From equation 2.1, with 500V applied to the electrodes, the normal force generated is:

$$F_{normal} = \frac{(283 \times 10^{-4}) \times (8.85 \times 10^{-12}) \times (500)^2}{2 \times (0 + 2 \times (6 \times 10^{-6})/3.2)^2} = 2255\text{N} \quad (2.2)$$

¹ The thickness of aluminum and mylar is calculated as follows: using a four point resistance measurement, the resistance of the aluminum sheet was measured. Then, thickness of the aluminum was calculated. The foil was weighed, and the corresponding mylar thickness was calculated.

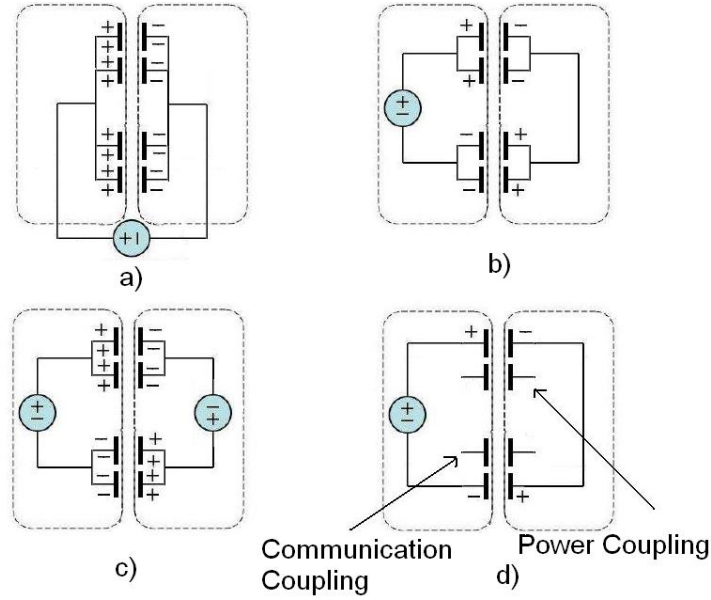


Fig. 2.6: Various methods to excite latches.

This calculation assumes that the applied voltage is high enough so that the electrodes conform to each other completely and there is no separation between them. In general, to get the maximum force, we would like to increase the voltage up to just below the level at which dielectric breakdown occurs ²

The shear force due to friction, which is the force the latch can withstand before disengaging, is:

$$F_{shear} = F_{normal} * \mu_{mylar-on-mylar} = 451N \quad (2.3)$$

Here, $\mu_{mylar-on-mylar} = 0.2$ [1].

Unlocking the latch is achieved by draining the charge on the faces of the adjacent robots. Our experiments have shown that over time, as the latch is engaged and disengaged again and again, a small fixed charge accumulates on the dielectric. Even after the charge across adjacent pairs of electrodes has been drained, residual charge is present due to trapped space charge [2]. This is particularly true when, as in our case, the dielectric has internal structural defects where charge is trapped. Since the dielectric has a high resistance, the charge trapped in the defects of the material remains even after the electrodes has been drained.

² Experiments have shown that the dielectric breakdown begins to occur at $\approx 850V$.

If not taken care of, this residual charge requires some force to separate the latch. This can be solved in two ways. First, dielectrics with less structural defects (e.g., oxide based thin-films) can be used. Second, the polarity of the applied voltage can be switched every time the latch is engaged. By reversing the polarity of the applied voltage, opposite polarity charge gets trapped each consecutive cycle, and they cancel out each other's effect.

To ease latch disengagement, each electrode surface is designed to have a slight release angle of 5 degrees. This release angle introduces a small amount of the peeling effect mentioned above, and as a result, although a high force is maintained when the electrodes are charged, the latch disengages easily—even if there is residual charge present after draining the capacitor.

2.2 Evaluation of the Macro-scale Electrostatic Latch

Experiments were done in which latch force measurements were taken with varying voltages applied to the electrodes. At each voltage, the latched was forced apart with an increasing load until disengagement, and the amount of load that caused disengagement was recorded. Figure 2.7 compares the theoretical and measured latch force.

Experimental data shows that at 500V, the measured force is significantly lower than the theoretical value, by a factor of three. Moreover, the measured force graph grows slower than $F = kV^2$ at smaller voltages, but starts to grow faster as the voltage reaches $\approx 400V$. This is due to the assumption in the theoretical force calculation that there is no separation between electrodes, i.e., the analysis assumes perfect electrode conformance. However, the electrode conformance is directly related to the force generated and thus directly to the applied voltage. We see that the electrodes do not conform well when the applied voltage is below 400V. Once the applied voltage reaches 400V, the electrodes conform much better and one can see that the measured force begins to grow as fast as the predicted force.

Although the measured force is in the range of hundreds of Newtons and is suitable for macro-scale modular robotics applications, it is still significantly lower than the theoretical value. This is due to several factors:

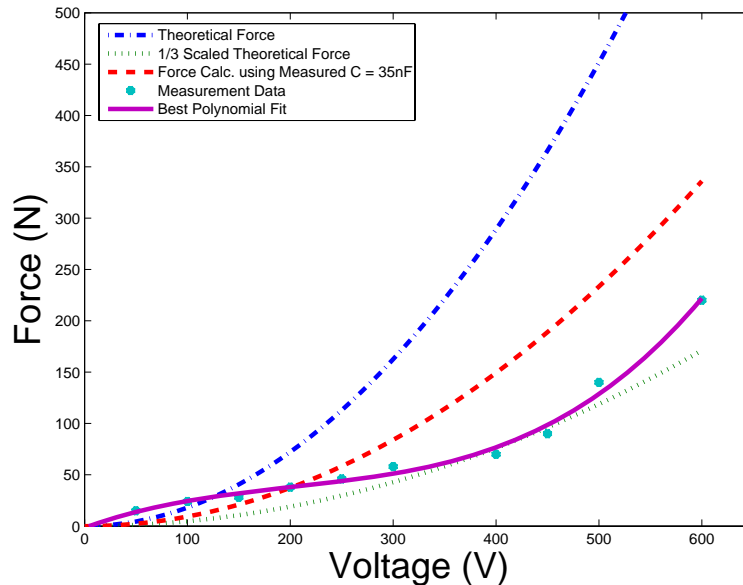


Fig. 2.7: Latch force versus applied voltage.

- The release angle designed to ease latch disengagement introduces the highly nonlinear peeling effect, which causes a decrease in the adhesion force. We observed reduced force for bigger release angles, however, having no release angle causes difficulty in mechanical latch disengagement³.
- As trapped charge builds up over time, the polarity of excitation is switched to get rid of the trapped charge. However, some amount of trapped charge is always present, which reduces repeatability of experiments and introduces significant measurement error.
- We observed that as the electrodes conform, due to the high electrostatic pressure, wrinkles form on the foils, thus, the effective area in Equation 2.1 is actually less than the geometrical value.
- The analysis assumes that the separation L between electrodes is zero; this might not be the actual case as there is not a simple way to tell whether air is trapped in between electrodes; which might also explain the wrinkles we observe in the face.
- Experiments revealed that the characteristics of the latch change with how tightly the foil is attached

³ It is conceivable to design a passive or active mechanism that changes the release angle on disengagement. However, such mechanism would increase the complexity of the latch.

to the panel. When it is too tight the foil on the panel cannot conform to the adjacent foil ⁴.

The capacitance between the electrodes of two faces was also measured, when the latch is engaged. As predicted, the capacitance measured when the electrodes are charged (with 500V) is significantly higher ($C \cong 35nF$) than when they are uncharged, but in contact with each other ($C \cong 8nF$). The measured capacitance is also lower than the theoretical value of $C = 68nF$ by a factor of ≈ 2 . This phenomena arises from the last four factors described above. (The first of the factors, the release angle, is strictly related to the force generated, not the capacitance.)

Figure 2.7 also shows the theoretical force that is calculated by extracting the effective area from the capacitance measurement. Since the measured force is less than this force, it can be concluded that the factors that do not change the capacitance but the force (i.e., release angle) have significant effects.

2.3 Electrostatic Latches at the Micro-scale

In this section we discuss the feasibility of using similarly designed latches at smaller scales (i.e. micrometers). The main question involved in using this design at smaller size scales is whether the conforming property of the flexible foil still exists, since this property is what actually creates the adhesion. To determine whether the material and electrostatic properties at the macro-scale still hold in the micro-scale, we investigated a model as shown in Figure 2.8. It is assumed that two square plate electrodes having the dimensions shown are charged with voltage V at the macro-scale. For the MEMS scale model, we scale the dimensions equally with a linear factor α and scale the voltage separately with factor κ , where $\alpha < 1$ and $\kappa < 1$.

To simplify the analysis we assume that only one electrode is flexible and conforming, while the other is rigid. Also, the dielectric coating and the metal layer are modeled with a single layer plate. These assumptions are both conservative and reasonable—experiments at the macro-scale show that the latch is effective even when only one electrode is flexible, e.g., a rigid aluminum sheet and a flexible foil-mylar electrode create significant shear forces ⁵.

⁴ Our current manufacturing process does not allow us to accurately repeat or measure the foil tightness.

⁵ This configuration is especially desirable since the effective separation is half (only a single layer of dielectric coating), and

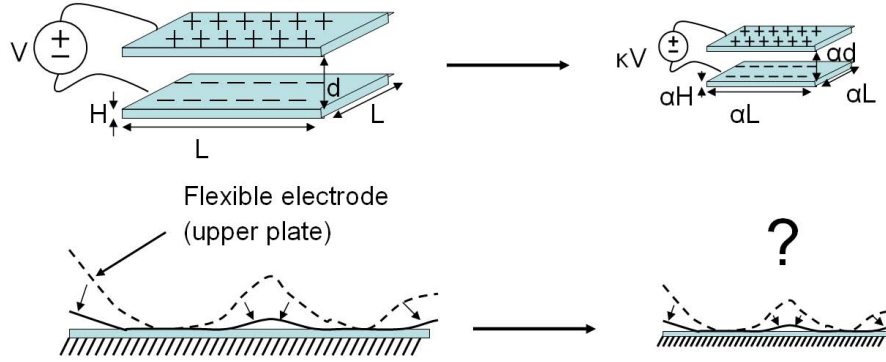


Fig. 2.8: Scaling down electrostatic latching.

The square plate that is rigidly attached at all sides bends in the presence of uniform pressure P according to equation 2.4 [11]:

$$P = \left\{ \frac{3\pi^2}{2} \left[\frac{\sigma_0 H}{L^2} \right] + \frac{2\pi^4}{3} \left[\frac{EH^3}{(1-v^2)L^4} \right] \right\} w + \frac{\pi^4(7-2v)(5+4v)}{128(1+v)} \left[\frac{EH}{(1-v)L^4} \right] w^3 \quad (2.4)$$

Here, w is a geometrical term that represents the deflection of the center of the plate. E is the Young's modulus of the material, σ_0 is the residual stress that is created due to the manufacturing process, v is the Poisson's ratio, H is the thickness of the plate, L is the side length of the square plate.

The shape function of the plate is given in equation 2.5 and Figure 2.9 shows the bent plate.

$$w_c = \frac{w}{4} \left[1 + \cos\left(\frac{2\pi x}{L}\right) \right] \left[1 + \cos\left(\frac{2\pi y}{L}\right) \right] \quad (2.5)$$

For our analysis, w is the geometrical term that represents how much the plate bends, which is also the measure of how much the plate can conform. Rather than the exact solution, we are mainly interested in the dependency of w on dimensions and voltage. Also, since we would like to focus on the case where w is relatively large, the w^3 term becomes dominant compared to the w term. Therefore, we will only consider the cubic (w^3) term in Equation 2.4. In the model described above, the pressure is the electrostatic force per unit area, with the simplifying assumption that it is uniform and does not change as the plate bends. Then, the force created is four times the force created when two layers of dielectric material is present. However, this configuration contradicts with the argument of having genderless faces and increases the complexity of the latch.

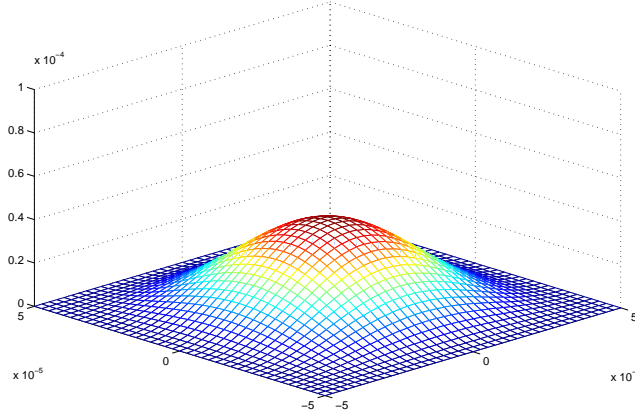


Fig. 2.9: Plate bending with uniform pressure (units not important).

considering only the second term in equation 2.4, the resulting dependency is:

$$P = K \frac{H}{L^4} w^3 = P_{electrostatic} = \frac{1}{2} \frac{V^2}{d^2} \quad (2.6)$$

$$K \frac{H}{L^4} w^3 = \frac{1}{2} \frac{V^2}{d^2} \quad (2.7)$$

$$w^3 = \frac{1}{K} \frac{L^4}{H} \frac{V^2}{d^2} \quad (2.8)$$

Here, $K = \frac{\pi^4(7-2\nu)(5+4\nu)E}{128(1+\nu)(1-\nu)}$.

At the MEMS scale, we assume all dimensions are scaled with α and voltage is scaled with κ . Then, we have:

$$w_{scaled}^3 = \frac{1}{K} \frac{\alpha^4 L^4}{\alpha H} \frac{\kappa^2 V^2}{\alpha^2 d^2} = \alpha \kappa^2 w^3 \quad (2.9)$$

$$w_{scaled} = \sqrt[3]{\alpha \kappa^2} w \quad (2.10)$$

Ideally, we would like to have $w_{scaled} = \alpha w$, since we would like to have the MEMS scale plate bend

the same way as the macro-scale plate, which will ensure similar conformance at the MEMS scale.

According to Equation 2.10, to have $w_{scaled} = \alpha w$, the condition is $\kappa = \alpha$. This implies that to have the electrostatic latching work the same way it does at the macro-scale, if all the dimensions are scaled down with a factor, the applied voltage must also be scaled down with the same factor. If this condition is satisfied, the bending happens in similar proportion to the macro-scale version, confirming that electrostatic latching mechanism scales.

Finally, scaling the applied voltage with the same factor also ensures that the magnitude of the electric field created $|E| = V/d$ stays constant, which is crucial in preventing dielectric breakdown.

In addition to the assumptions made above, MEMS scale latches require the consideration of additional factors. MEMS thin film materials might have characteristics which are different from their macro-scale -bulk- counterparts. An example of this is the dielectric field strength of silicon dioxide (SiO_2). Thin film silicon dioxide tends to be much more resistant to dielectric breakdown, compared to bulk silicon dioxide. Thus, for example, a MEMS scale electrostatic latch utilizing silicon dioxide as a dielectric must consider this drastic change in the material property. Designing appropriate latch behavior at MEMS scale might require the use of non-traditional values for properties such as permittivity, Poisson's ratio and Young's modulus. Furthermore, environmental factors such as dust require much greater attention at smaller scales.

2.4 Summary

The demonstrated macro-scale electrostatic latch performs as desired, and the MEMS scale latches are promising.

The adhesion force generated per cm^2 of face area is $0.6N$, when $500V$. This corresponds to $0.53N/cm^2$ of electrode area. Since the electrode is normal to the plane of the face this gives the latch designer an additional parameter to work with when designing a face. The electrodes are versatile in their arrangement on the latch and can be made self-aligning. The energy needed to lock and unlock the latches is very low—the theoretical value is the energy stored on the capacitor formed by the latch electrodes, which is $W = 1/2CV^2 = 8.5mJ$. This is the amount of energy required to lock the latch once. The latch consumes no power once locked, and the stored energy may even be partially recovered.

In short, the latch is powerful, power efficient and self aligning. In addition, the analysis reveals that the same idea can be applied to smaller scale latches. Making use of shear forces, the latch generates forces high enough for macro-scale modular robotics applications. In Chapter 4 a modular robot that integrates the electrostatic latches is discussed.

3. POWER TRANSFER

In this chapter we describe how to transfer power through an ensemble using capacitive coupling between adjacent modules. Much as a transformer uses an electromagnetic coupling between coils to transmit power across an insulator, a pair of capacitors can be used to carry energy across a non-conducting gap. A potential advantage of capacitive transfer is that it should not require the high mass- or spring-induced contact forces typically needed for DC connectors to break through oxide layers, counteract surface roughness, or operate in dirty environments.

The following analysis has been done to demonstrate the potential for power transport between adjacent modules via their electrostatic latches using AC excitations. Figure 3.1 illustrates the general approach used. Note that neither a common ground nor any non-capacitively-coupled connections between modules are required.

3.1 Feasibility of Power Transfer

This section includes the analysis on the feasibility of transferring power across a capacitive coupling. Figure 3.2 shows the diagram of the circuit representing the model that is analyzed.

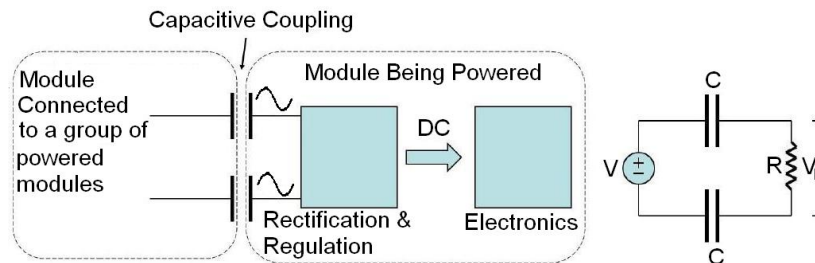


Fig. 3.1: Power transfer between robots.

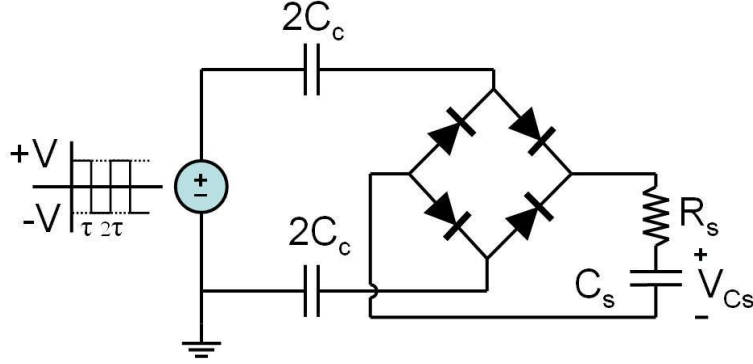


Fig. 3.2: A model for power transfer between robots; $2C_c$'s denote the coupling capacitors while C_s denotes the storage capacitor.

For simplicity, a square wave generator is used as the voltage source on the source module. The generated voltage alternates between $+V$ and $-V$. This source is coupled to the target module through two capacitors, each of value $2C_c$. On the target module, there is a full wave rectifier built out of 4 diodes, and the module's storage capacitor C_s . Also, there is a resistance R_s that represents the lumped series resistance of the circuit.

The purpose of this analysis is to determine how much voltage (thus energy) can be built up on the target capacitor C_s . However, as the following analysis will reveal, a voltage level of V can always be reached on C_s given *enough* time, thus, a more realistic question is how much time would it take to reach a certain voltage level. In this analysis, emphasis is given to charge time, t_{CHARGE} , which is the time it takes to charge C_s to a certain level. Also, another important measure of feasibility is the power transfer efficiency, which is also discussed.

In this analysis, for simplicity, the rectifying diodes are assumed to be ideal, i.e., the turn on voltage $V_{ON} = 0^+$, and the forward resistance is $R_{FW} = 0$ ¹.

Initially, at time $t = 0$, neither the coupling capacitors nor the storage capacitor are charged. At $t = 0^+$, the voltage across the source becomes $+V$. The storage capacitor begins to charge. Eventually, the voltage reaches its final value, which can be calculated using the voltage division law for capacitors. The final voltage on C_s , $V_{C_s n}$, where $n \in \mathbb{Z}^+$ denotes the number of source voltage transitions, is:

¹ For $V_{ON} \neq 0$, it is easy to show that the analysis yields the same results when the source voltage is assumed to be $V_{source} = V + 2V_{ON}$. Also, the effect of R_{FW} can be taken into account in the lumped series resistance R_s .

$$V_{C_s1} = V \frac{C_c}{C_c + C_s} \quad (3.1)$$

The period of the square wave is 2τ . It is assumed that τ is much larger than the time constant of the circuit. This, in effect, is the equivalent of the assumption that R_s is *very small*, thus, when the voltage source is switched from 0 to $+V$, the storage capacitor voltage V_{C_s} reaches it's final value immediately.

At $t = \tau^+$, the source voltage is switched to $-V$, and thus, the storage capacitor is charged to:

$$V_{C_s2} = V \frac{3C_c C_s + C_c^2}{(C_c + C_s)^2} \quad (3.2)$$

This analysis can be extended to solve the value of the voltage on storage capacitor after n transitions ($t = n\tau^+$), in relation to the voltage level after $n - 1$ transitions:

$$V_{C_s n} = V \frac{2C_c}{C_c + C_s} + V_{C_s(n-1)} \frac{C_s - C_c}{C_c + C_s} \quad (3.3)$$

The relation given in Equation 3.3, can be used to construct the equation relating the storage capacitor voltage after n transitions in relation to the source voltage V and V_{C_s1} :

$$V_{C_s n} = V \frac{2C_c}{C_c + C_s} \left[1 + \left(\frac{C_s - C_c}{C_c + C_s} \right) + \left(\frac{C_s - C_c}{C_c + C_s} \right)^2 + \dots + \left(\frac{C_s - C_c}{C_c + C_s} \right)^{n-2} \right] + V_{C_s1} \left(\frac{C_s - C_c}{C_c + C_s} \right)^{n-1} \quad (3.4)$$

Another assumption can be made to further simplify Equation 3.4: the storage capacitance C_s is larger than the effective coupling capacitance C_c . In Chapter 2, it is demonstrated that the coupling capacitance is in the order of nanoFarads. However, since the power requirements are in the order of milliJoules, it is fair to assume that the storage capacitor on any module would be in the order of milliFarads, thus $C_s > C_c$.

With this assumption, Equation 3.4 simplifies to:

$$V_{C_s n} = V \left[1 - \left(\frac{C_s - C_c}{C_c + C_s} \right)^{n-1} \right] + V_{C_s1} \left(\frac{C_s - C_c}{C_c + C_s} \right)^{n-1} \quad (3.5)$$

An important property of this relation is that as time passes, the storage capacitor voltage $V_{C_s n}$ reaches V , that is, $\lim_{n \rightarrow \infty} V_{C_s n} = V$. Therefore, it can be concluded that any voltage level up to the source voltage can be achieved at the target capacitor, given enough time.

Equation 3.4 also shows that for the case where $C_c > C_s$, the storage capacitor reaches a voltage level above V at $n = 2$. For larger values of n , the solution is not valid, since the equation does not correspond to the actual case where none of the diodes are turning on at any time after $n = 2$. This case is out of the scope of our analysis.

The results show that depending on the values of C_s and C_c , the storage capacitor voltage can reach value up to V , provided that n is large enough. For the case where $C_s = 1mF$ and $C_c = 10nF$, to reach 95% of the source voltage V , the number of transitions required is $n = 150,000$. For a source excitation frequency of $1MHz$, the target voltage is reached in $t_{CHARGE} = 75milliseconds$.

Equation 3.4 suggests that to further decrease the charge time of the storage capacitor, t_{CHARGE} , the source frequency must be increased. However, an exact solution for charge time requires us to more realistically represent the situation, i.e., where there is a finite lumped series resistance R_s . To represent R_s , Equation 3.3 can be modified as:

$$V_{C_s n} = V \frac{2C_c}{C_c + C_s} (1 - e^{-\frac{(C_s + C_c)}{R_s C_c C_s} \tau}) + V_{C_s (n-1)} \frac{C_s - C_c + 2C_c e^{-\frac{(C_s + C_c)}{R_s C_c C_s} \tau}}{C_c + C_s} \quad (3.6)$$

Similarly, Equation 3.5 can be modified as:

$$V_{C_s n} = V \left[1 - \left(\frac{C_s - C_c + 2C_c e^{-\frac{(C_s + C_c)}{R_s C_c C_s} \tau}}{C_c + C_s} \right)^{n-1} \right] + V_{C_s 1} \left(\frac{C_s - C_c + 2C_c e^{-\frac{(C_s + C_c)}{R_s C_c C_s} \tau}}{C_c + C_s} \right)^{n-1} \quad (3.7)$$

which further simplifies to:

$$V_{C_s n} = V \left[1 - \left(\frac{C_s - C_c + 2C_c e^{-\frac{(C_s + C_c)}{R_s C_c C_s} \tau}}{C_c + C_s} \right)^{n-1} \left(1 - \frac{C_s}{C_c + C_s} (1 - e^{-\frac{(C_s + C_c)}{R_s C_c C_s} \tau}) \right) \right] \quad (3.8)$$

Note that, again, $\lim_{n \rightarrow \infty} V_{C_s n} = V$.

The figure of merit of this analysis, which is the charge time t_{CHARGE} , can be solved analytically using Equation 3.8. Defining κ as the percentage of source voltage V that is desired to be achieved on the storage capacitor, the t_{CHARGE} is:

$$t_{CHARGE} = \frac{1}{2f} \left(\frac{\ln \left(\frac{1-\kappa}{1 - \frac{C_c}{C_c+C_s} e^{-\frac{(C_s+C_c)}{R_s C_c C_s 2f}}} \right)}{\ln \left(\frac{C_s - C_c + 2C_c e^{-\frac{(C_s+C_c)}{R_s C_c C_s 2f}}}{C_c + C_s} \right)} - 1 \right) \quad (3.9)$$

The variation of t_{CHARGE} with respect to different parameters is plotted in following Figure 3.3

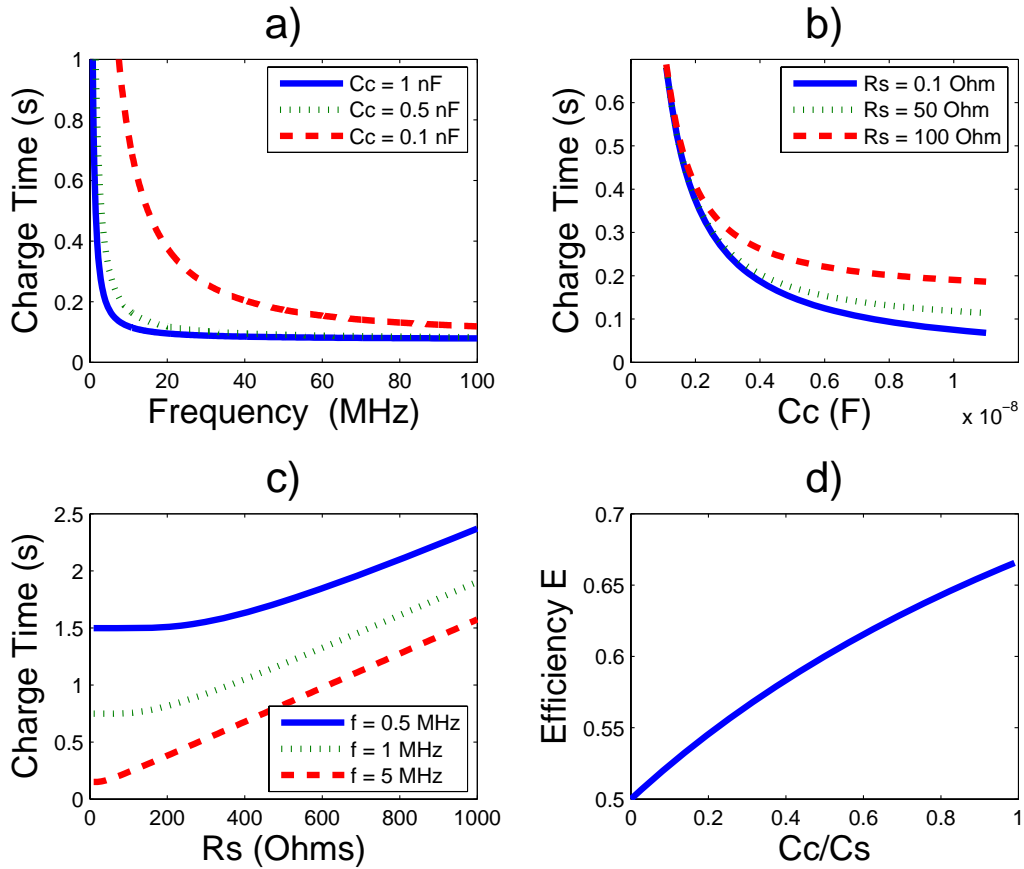


Fig. 3.3: a: Charge time versus frequency f of input square wave, b: Charge time versus coupling capacitance C_c , c: Charge time versus lumped series resistance R_s , d: Efficiency versus C_c/C_s ratio.

In Figure 3.3, the parameters are set as follows (unless varied): $C_c = 1 \times 10^{-9}F$, $C_s = 1 \times 10^{-3}F$, $R_s = 50\Omega$, $f = 1MHz$, $\kappa = 0.95$. This analysis shows that the charge time t_{CHARGE} decreases asymptotically as the frequency f or the coupling capacitance C_c is increased. In fact, it can be shown (using L'Hospital's Rule) that:

$$\lim_{f \rightarrow \infty} t_{CHARGE} = \frac{1}{2} R_s C_s \ln \left(\frac{C_s}{(C_c + C_s)(1 - \kappa)} \right) \quad (3.10)$$

Equation 3.10 shows that t_{CHARGE} decreases for smaller values of R_s . For better (faster) power transfer between modules, the coupling capacitance and the excitation frequency should be maximized while the lumped series resistance is kept minimal.

Another very important measure is the power transfer efficiency², E . When enough time passes, all the energy is stored on the storage capacitor C_s , $W_{C_s} = \frac{1}{2} C_s V_{C_s}^2$, and no energy is stored on coupling capacitor C_c , since $\lim_{n \rightarrow \infty} V_{C_c n} = 0$. However, to calculate the efficiency, the energy that is dissipated on the series resistance R_s , W_{R_s} , must be found. Then,

$$E = \frac{W_{Stored}}{W_{Total}} = \frac{W_{C_s}}{W_{C_s} + W_{R_s}} \quad (3.11)$$

To find W_{R_s} , the series resistance voltage V_{R_s} must be found. Using 3.5 and $V_{R_s}(t) = R_s C_s \frac{dV_{C_s n}}{dt}$, we get an expression for $V_{R_s}(t)$ after n transitions:

$$V_{R_s n}(t) = 2(V - V_{C_s(n-1)}) e^{-\frac{(C_s + C_c)}{R_s C_c C_s} t} \quad (3.12)$$

$$V_{R_s n}(t) = 2V \left(\frac{C_s - C_c + 2C_c e^{-\frac{(C_s + C_c)}{R_s C_c C_s} \tau}}{C_c + C_s} \right)^{(n-1)} \left(1 - \frac{C_s}{C_c + C_s} (1 - e^{-\frac{(C_s + C_c)}{R_s C_c C_s} \tau}) \right) e^{-\frac{(C_s + C_c)}{R_s C_c C_s} t} \quad (3.13)$$

The power and energy dissipated from n th to $(n + 1)$ th transition is:

² In our model the voltage source is assumed to be ideal; a square wave of any amplitude and frequency can be generated at no power cost. The source *does work* only when there is a current in the circuit, charging capacitors and dissipating power over R_s . This does not reflect the reality as any square wave generator would consume power even when it's terminals are not connected.

$$P_{V_{R_s n}}(t) = \frac{V_{R_s n}^2(t)}{R_s}, \quad W_{R_s n} = \int_0^\tau P_{V_{R_s n}}(t) dt, \quad (3.14)$$

And finally, the total energy dissipated on R_s is:

$$W_{R_s} = \sum_{i=1}^n W_{R_s i} \quad (3.15)$$

Using Equations 3.13, 3.14 and 3.15, the energy dissipated on R_s as $n \rightarrow \infty$ (or equivalently $t \rightarrow \infty$), and the efficiency E can be calculated as:

$$\lim_{n \rightarrow \infty} W_{R_s} = \frac{1}{2} V^2 \frac{C_s^2}{(C_c + C_s)}, \quad E = \frac{\frac{1}{2} C_s V^2}{\frac{1}{2} C_s V^2 + \frac{1}{2} V^2 \frac{C_s^2}{(C_c + C_s)}} = \frac{C_c + C_s}{C_c + 2C_s} \quad (3.16)$$

Figure 3.3d shows a plot of efficiency E versus changing C_c . It must be noted that the efficiency is bounded by $2/3$, as this is the case where $C_c = C_s$, and the analysis is not valid for $C_c > C_s$. For typical values of C_c and C_s given in Chapter 2, $E \cong 0.50$. Also, the efficiency is independent of R_s .

3.2 Summary

Using the electrodes on each face of the latch to transfer power between modules is an appealing solution.

The above model shows that for well-engineered values of parameters, power transfer between modules can be achieved in a reasonable time, for both macro and MEMS scale capacitive coupling. However, this model suffers from low power transfer efficiency. In an actual implementation of this model, the module-to-module power transfer efficiency would further decrease due to power dissipation at the source voltage generator, and other non-ideal effects.

A model based on the idea of charging a storage capacitor using a simple voltage source lacks the higher efficiencies required for transferring power through large ensembles of modules. Due to the loss at every interface, the total power requirements of the ensemble grow exponentially with the number of modules in the ensemble, when power is transferred to modules farther away through the modules that are in between the source and the target. For better power transfer efficiency, different circuit topologies, for example charge

pumps, must be investigated.

In addition to power transfer, another challenge for modular robotics is to design an efficient communication method between modules. Again, the capacitive coupling offers a solution. An AC excitation created at the source module can be sensed at the target module, through the coupling capacitors. Furthermore, in Chapter 2, it is demonstrated that it is possible to dedicate individual electrodes on each face to different purposes. While some electrodes are used for latching or power transfer, at the same time, some can be used to transfer data between modules. In fact, it is not hard to see how one can transfer power and communicate simultaneously, over the same coupling electrodes.

4. DEMONSTRATION CUBIC ROBOT

To demonstrate the ideas presented in the previous two chapters we designed and built a cubic lattice-style modular robot which uses electrostatic latching. The robot has a packing and gait similar to Rus and Vona's Crystalline Atom [9] and PARC's Telecube [12]. These modules reconfigure using an inchworm gait by expanding the connected faces of two neighboring modules so that one of them is pushed one block length across the assembly, and then contracting again to pull the next module forwards (Figure 1.1c shows a module in the middle of its movement operation). A video of the robot using its electrostatic latch is at www.cs.cmu.edu/~claytronics/iros07-latch.html.

This form factor has several desirable properties: the positions of modules are highly constrained by the cubic lattice which simplifies planning and mating; Rus and Vona [9] have demonstrated that with a sufficiently large meta module any arbitrary configuration of voxels is reachable; and modules can propagate through the center of an assembly allowing the system to reconfigure more quickly than systems where modules can only move along the surface of an assembly.

As it provides adhesion, power transfer and communication in a simple and robust package our electrostatic latch reduces the complexity of the entire system. By reducing the number of systems in each module we simplify fitting them within the available space, and enhance their manufacturability. This makes it feasible to produce larger numbers of modules and experiment with more interesting behaviors.

4.1 Actuation Subsystems

Our robot is composed of two active systems: an electrostatic latch that provides adhesion, and a modular worm drive assembly that expands and contracts the faces using a DC-motor. We use passive systems to provide alignment and to limit the extension of the faces to avoid the need for any further sensing or actuation

components.

4.1.1 Mechanical Actuation for Expansion and Contraction

The linear actuation subsystem drives arms attached to each face so that the opposing faces of the module can move from a fully contracted state (22cm between faces) to a fully expanded state (44cm between faces). Each face has its own dedicated, independently controlled worm drive housed in a modular tube. The arm attached to each face fits into this tube. The six tubes containing the face assemblies are bolted together to create the central frame for the robot as shown in Figure 1.1b.

4.1.2 Genderless Self-aligning Comb Latch

Although we could have used male and female mating latches, we used a genderless latch to reduce the number of components in the system and ease assembly. As shown in Figure 2.3, each face of the robot is corrugated in a radial comb pattern. The top of each comb terminates in a forty-five degree blade to provide passive self-alignment. The vertical faces of the combs have slots to the electrodes. Two faces mate tightly together to provide a rigid moment connection. The vertical faces of the combs have a five degree release angle to allow the faces to retract easily once the charge has been drained from the electrodes.

Each face has sixteen 3cm deep capacitive panels mounted on eight combs. We could have designed the latch with fewer larger combs; which would increase the amount of misalignment that could be passively corrected. However, this would increase the height of the blades and make it more difficult to achieve a compact gait that would clear neighboring latches. We choose to reduce the depth of the plates resulting in a more compact packing of the modules.

4.2 Impact of Latch on Overall Design

As with most robot designs, cubic lattice-style modular robots must balance a variety of sometimes conflicting design goals relating both to the performance of individual parts, and of the system as a whole. Here we describe how the features of our latch impact the design of the entire system:

Robust Docking: Other systems have used either mechanical or magnetic latches to connect and disconnect from neighboring modules. Both of these strategies have problems. Mechanical latches like Polybot's [13] tend to seize and fail to disengage under load unless they use very large, heavy motors relative to the size of the module like ATRON [8]. Switching permanent magnet latches like the TeleCube's [12] provide a limited amount of force, are heavy and require complex mechanical actuators. Our electrostatic latch provides a robust, lightweight electronically controlled mechanism for both latching to and unlatching from neighboring modules. When activated it provides a great deal of force, and when deactivated the two neighboring faces separate easily with little force.

As our electrostatic latch also provides power transfer and communication it allows us to use fewer discrete components than other systems which have separate subsystems to handle each of these functions. Our latch design lends itself to being inexpensively mass produced as it consists of only a single monolithic plastic frame with an array of electrodes and the wiring to connect them.

Passive Self-alignment: Although the rigid packing of modules within a crystalline lattice helps to align modules there is inevitably some degree of misalignment that must be corrected when two modules mate. The shape of our latches forces the combs into alignment as they move closer together. This passive self-aligning mechanism is designed to correct misalignments of up to 18% of the width of a face, or a rotational misalignment of up to 40 degrees. We believe that this is a significant improvement over other systems and one of the strongest points of our design.

This robust passive self-alignment mechanism obviates the need for extra sensing components to detect when modules are near enough to actuate the latch. The arms of the neighboring modules are simply driven towards each other until a current sensor on the motor power line indicates that there is mechanical resistance, and then the electrodes are charged to lock the faces together.

Reducing System Weight: Our electrostatic latching system greatly reduces the overall weight of our modules compared to mechanical latches such as ATRON's [8] and permanent magnetic latches such as the TeleCube's [12], as it requires neither motors nor magnets. It also allows a better latch to total weight ratio. We compare the weight of the entire six faces and the electronics for driving the electrodes with the weight of the entire module. Measured this way our latch is still only 40% of the weight of the entire module, while

the ATRON's latches account for 60% of the weight of the entire module.

4.3 *Summary*

We evaluated the latch design using an 3.5kg modular robot. The robot's inchworm gait requires that the latch robustly lock onto another robot and move it three body lengths, in order to be able to move in a cubic lattice. The latch demonstrated was able to provide self-alignment and easy engagement between robots. As one robot lets go of another the latch is easily disengaged. Finally, the latch was strong enough to pull another robot along.

5. CONCLUSIONS

The electrostatic latch described in this report delivers on its promise of providing robust adhesion, self-alignment, easy detachment all for less weight and power than used in other designs. The key insight that makes the latch so effective is capitalizing upon shear force between flexible, capacitively coupled electrodes. This avoids the negative effects of peeling, while still maintaining the tolerance for initial air gaps and dust particles of flexible electrodes. Its ability to form the basis of inter-module communication and power transfer make it especially attractive in the context of modular robotics, as it eliminates additional connections for those purposes. Our cubic robot demonstrates that this reduction in complexity simplified the design and construction of a modular robotic system.

BIBLIOGRAPHY

- [1] http://www.goodfellow.com/csp/active/static/e/polyethylene_terephthalate.html.
- [2] L. Dissado, G. Mazzanti, and G. C. Montanari. The role of trapped space charges in the electrical aging of insulating materials. *IEEE Transactions on Dielectrics and Electrical Insulation*, 4(5):496–506, 1997.
- [3] Toshio Fukuda, Tsuyoshi Ueyama, Yoshio Kawauchi, and Fumihito Arai. Concept of cellular robotic system (cebot) and basic strategies for its realization. *Comput. Electr. Eng.*, 18(1):11–39, 1992.
- [4] Mustafa Emre Karagozler, Brian Kirby, W.J. Lee, Eugene Marinelli, T.C. Ng, Michael Weller, and Seth Copen Goldstein. Ultralight modular robotic building blocks for the rapid deployment of planetary outposts. In *Revolutionary Aerospace Systems Concepts Academic Linkage (RASC-AL) Forum 2006*, Cape Canaveral, FL, May 2006.
- [5] K. Kotay, D. Rus, M. Vona, and C. McGray. The self-reconfiguring robotic molecule. In *IEEE International Conference on Robotics and Automation (ICRA)*, pages 424–31, 1998.
- [6] S. Murata, H. Kurokawa, and S. Kokaji. Self-assembling machine. In *Proc. IEEE Int. Conf. Robotics and Automation*, pages 441–8, 1994.
- [7] Satoshi Murata, Eiichi Yoshida, Akiya Kamimura, Haruhisa Kurokawa, Kohji Tomita, and Shigeru Kokaji. M-tran: Self-reconfigurable modular robotic system. *IEEE/ASME Transactions on Mechatronics*, 7(4):431 – 441, December 2002.
- [8] Esben Hallundbaek Ostergaard, Kristian Kassow, Richard Beck, and Henrik Hautop Lund. Design of the atron lattice-based self-reconfigurable robot. *Auton. Robots*, 21(2):165–183, 2006.

-
- [9] Daniela Rus and Marselette Vona. Crystalline robots: Self-reconfiguration with compressible unit modules. *Autonomous Robots*, 10(1):107–124, 2001.
- [10] Behnam Salemi, Mark Moll, and Wei-Min Shen. SUPERBOT: A deployable, multi-functional, and modular self-reconfigurable robotic system. In *iros-06*, Beijing, China, oct 2006. To appear.
- [11] Stephen D. Senturia. In *Microsystem Design*, pages 255–258. Kluwer Academic Publishers, 2002.
- [12] J.W. Suh, S.B. Homans, and M. Yim. Telecubes: mechanical design of a module for self-reconfigurable robotics. In *Proc. of the IEEE Int’l Conference on Robotics and Automation (ICRA)*, volume 4, pages 4095–101, 2002.
- [13] M. Yim, D.G. Duff, and K.D. Roufas. Polybot: a modular reconfigurable robot. In *IEEE International Conference on Robotics and Automation (ICRA)*, volume 1, pages 514–20, 2000.